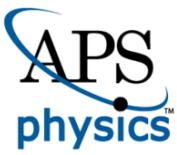

Probing many-body interactions in the cyclotron resonance of math xmlns="http://www.w3.org/1998/Math/MathML">mi>h/mi> /math>-BN/bilayer graphene/math xmlns="http://www.w3.org/1998/Math/MathML">mi>h/mi> /math>-BN

Rai Moriya, Sabin Park, Satoru Masubuchi, Kenji Watanabe, Takashi Taniguchi, and Tomoki Machida

Phys. Rev. B **104**, 245137 — Published 27 December 2021

DOI: 10.1103/PhysRevB.104.245137

Probing many-body interactions in the cyclotron resonance of *h*-BN/bilayer graphene/*h*-BN

Rai Moriya[1,*], Sabin Park[1], Satoru Masubuchi[1], Kenji Watanabe[2], Takashi Taniguchi[3,1], and Tomoki Machida[1,*]

[1] *Institute of Industrial Science, University of Tokyo, 4-6-1 Komaba, Meguro, Tokyo 153-8505, Japan*

[2] *Research Center for Functional Materials, National Institute for Materials Science, 1-1 Namiki, Tsukuba 305-0044, Japan*

[3] *International Center for Materials Nanoarchitectonics, National Institute for Materials Science, 1-1 Namiki, Tsukuba 305-0044, Japan*

Unlike a conventional two-dimensional electron gas system, which has parabolic band structure, the non-parabolic band dispersion of mono- to few-layer graphene violates Kohn's theorem. Thus, Landau levels (LLs) in graphene are sensitive to many-body interactions. This modifies the LL spacing, depending on the location of the Fermi energy (E_F). Such effects have been extensively studied in *h*-BN/monolayer graphene (MLG)/*h*-BN through observation of inter-LL optical transitions known as cyclotron resonances (CRs). However, thus far, the influence of many-body interactions on the CR of bilayer graphene (BLG) has been rarely studied, even though BLG also possesses non-parabolic band dispersion. Here, we investigate CR in the *h*-BN/BLG/*h*-BN structure via magneto-photothermoelectric measurements under infrared laser irradiation. This method enables sensitive detection of cyclotron resonances while tuning E_F of BLG. The CR magnetic field value shifted significantly

when E_F of BLG approached the charge neutrality point (the Dirac point, DP). We attribute this to a change in the Fermi velocity of BLG near the DP, which occurs as a result of many-body interactions.

---

*E-mail: moriyar@iis.u-tokyo.ac.jp; tmachida@iis.u-tokyo.ac.jp

The unique band structure of Landau-quantized mono- to few-layer graphene has been probed via the study of inter-Landau-level transitions, which are also known as cyclotron resonances (CRs) [1-10]. Unlike electrical transport measurements, in which transport properties at the Fermi level are detected, CR measurement enables the detection of properties away from the Fermi level. Therefore, this method is a very powerful tool for investigating Fermi-level-dependent changes in CR transitions, revealing variation in the inter-Landau-level spacing as a function of Fermi energy. Pioneering research has been carried out recently on high-quality monolayer graphene encapsulated by the insulator *h*-BN and revealed the presence of a significant many-body interaction that modulates the energy gap for CR transitions, depending on the Fermi level of the graphene layer [5,6]. This finding raised a series of related questions that have been examined in theoretical as well as experimental studies [11,12]. This many-body interaction effect is in striking contrast to the behavior of a conventional two-dimensional electron gas system, which has a parabolic band structure and CR that is insensitive to many-body interactions, in accordance with Kohn's theorem [13]. Graphene provides a novel platform to investigate the correlation between CR and many-body interaction. Particularly, in bilayer graphene (BLG), the many-body interaction is expected to contribute to CR because BLG also possesses non-parabolic band dispersion (which is sometimes referred to as massive Dirac band structure) [11,13,14]. However, the effect of many-body interaction on CR has rarely been investigated in the case of BLG. Interaction-driven reconstruction of the band structure has been observed in suspended BLG at zero magnetic field [15] and recent studies on the CR measurement of BLG revealed unconventional selection rules and discussed the possible contribution of many-body interaction [16]; however, no detailed

investigation has been presented thus far. Herein, we demonstrate the influence of many-body interactions on the LLs of BLG encapsulated by *h*-BN via magneto-photothermoelectric effect measurements.

A schematic illustration of the device structure investigated in this study is presented in Fig. 1(a). A two-terminal *h*-BN/BLG/*h*-BN structure was placed on a 290-nm SiO_2/highly doped Si substrate with Au/Cr electrodes. The channel region was shaped into a mesa structure by reactive ion etching (RIE) with a mixture of CF_4, Ar, and O_2. The doped Si was used as a back gate to control the carrier density of the BLG. The sample was placed in a liquid He cryostat with a variable-temperature insert and superconducting magnet. In the experimental arrangement, light from a wavelength-tunable CO_2 laser (Access Laser Inc. Merit-G, wavelength λ, 9.24–10.675 μm) was delivered to the sample using a hollow-core optical fiber and light pipe; note that the laser light reaching the sample was unpolarized. Thus, the photovoltage generated between the two electrodes of the BLG was measured under low-temperature and high-magnetic-field conditions [3,4,7,8].

The two-terminal conductance G was measured during the application of an AC current (I_{ac} = 10 nA) at a frequency of 18 Hz as its carrier density n (tuned by the back-gate voltage V_{BG}) was varied at 2.0 K, and the results are shown in Fig. 1(b). This plot indicates ambipolar characteristics for the conductance. The photovoltage, V_{ph}, was measured during irradiation, as illustrated in Fig. 1(a). For these measurements, we used a lock-in detection method such that the CO_2 laser was modulated by an optical chopper at a frequency of 18 Hz and the photovoltage was measured using a lock-in amplifier. The variation of V_{ph} with n measured at zero magnetic field and T = 2.0 K under irradiation at λ = 10.675 μm is shown in Fig. 1(c). In this plot, V_{ph} has a signal with a peak and dip

structure centered around $n = 0$, the charge neutrality point (Dirac point, DP), in contrast to the dip structure shown in Fig. 1(b). The peak and dip at the DP is reminiscent of the photothermoelectric effect [3,4]. It has been established that the photothermoelectric effect is the dominant mechanism for photovoltage generation in graphene devices [3,4,7]. In this mechanism, light absorption by graphene first increases its electron temperature and creates a temperature gradient at the junction between the graphene channel and the graphene in contact with the metal electrode. Subsequently, this induces a thermoelectric voltage at the junction between the graphene channel and the metal-covered graphene. Thus, the n-dependent shape of V_{ph} reflects the shape of the thermoelectric coefficient of BLG, which has a peak and dip structure near the DP [3,4,8,17-19]; this is consistent with our observations as shown in Fig. 1(c).

Next, the dependence of V_{ph} on the magnetic field B at fixed $n = 5.94 \times 10^{10}$ cm^{-2}, $\lambda = 10.675$ μm, and $T = 2.0$ K was measured, and the results are shown in Fig. 1(d). A series of peaks observed in the high-B region are indicated by arrows in the figure. The variation of V_{ph} with B and n is shown as a 2D plot in Fig. 1(e), where a series of resonances is also apparent. We attributed these signals to BLG cyclotron resonances. In Fig. 1(f), the energies of Landau levels with different indices N are plotted with respect to B. Considering the irradiation energy E_{ph} at $\lambda = 10.675$ μm ($E_{ph} = 116.14$ meV) and the $\Delta|N| = \pm 1$ selection rule for cyclotron resonance transitions, several different transitions, namely T_3–T_6, should be observable within the magnetic field range we studied. Each transition consists of two different channels: the T_3 transition ($N = -2 \rightarrow +3$ and $N = -3 \rightarrow +2$ channels), the T_4 transition ($N = -3 \rightarrow +4$ and $N = -4 \rightarrow +3$), the T_5 transition ($N = -4 \rightarrow +5$ and $N = -5 \rightarrow +4$), and the T_6 transition ($N = -5 \rightarrow +6$ and $N = -6 \rightarrow +5$). Because of the electron–hole

asymmetry in the band dispersion of BLG [1,20,21], for the same $|N|$, the LL energies of electrons (positive N) are always greater than those of holes (negative N) for $N > 2$. For the T_3 transition, the transition channel corresponding to $N = -2 \rightarrow +3$ appeared at lower B field with respect to that for $N = -3 \rightarrow +2$. Similarly, for the T_4 transition, $N = -3 \rightarrow +4$ appeared at lower B field values than $N = -4 \rightarrow +3$, and so on. Note that in principle more transitions can be identified, such as T_7 and T_8, at low B; however, these signals are too small to distinguish. For this reason, we discuss the CR transitions T_3 to T_6 in the present manuscript.

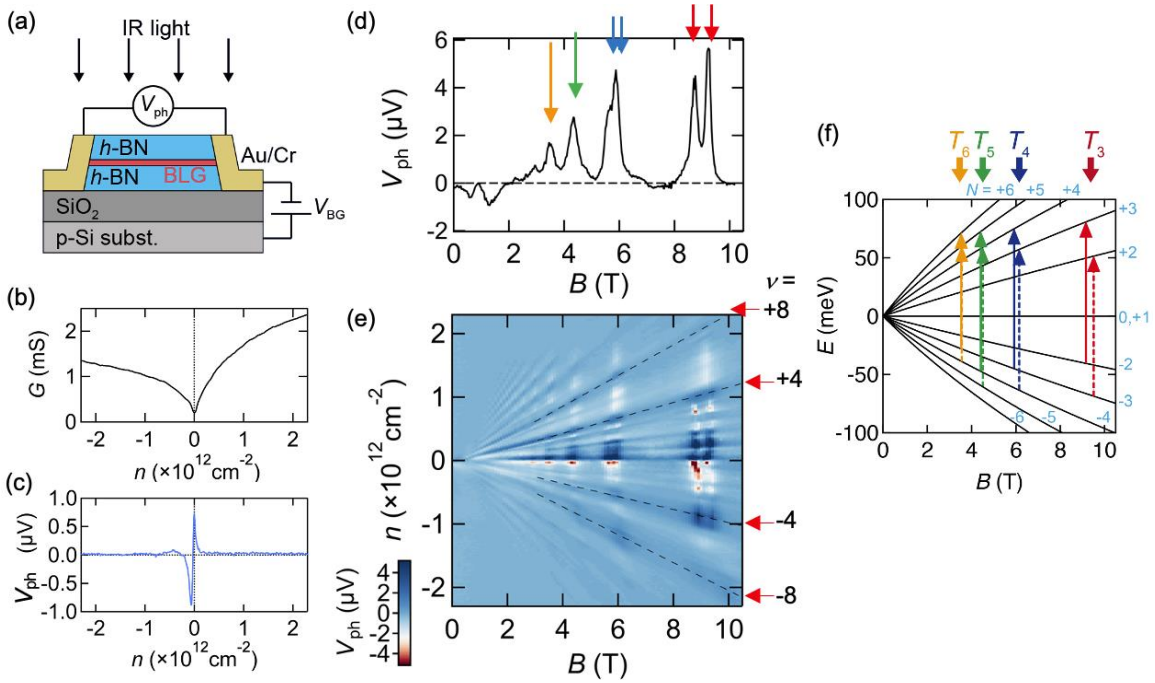

Figure 1. (a) Schematic illustration of device structure. (b) Two-terminal conductance *G* as a function of carrier density *n*. (c) Photovoltage V_{ph} as a function of *n*. (d) V_{ph} as a function of magnetic field *B* at fixed *n* ($n = 5.94 \times 10^{10}$ cm^{-2}). (e) V_{ph} as a function of *B* and *n*. (f) Energies of LLs with LL indices in the range of $N = -6$ to +6; cyclotron resonance transitions T_3 to T_6 are indicated by arrows. All the experimental data shown in this figure were acquired at a temperature of 2.0 K.

Next, in Figs. 2(a) and 2(b) we present detailed V_{ph} mapping for the T_3, T_4, and T_5 transitions as a function of *B* and *n*; the black dashed straight lines in these figures are a guide to the eye. Comparing the experimental data with these lines reveals that the magnetic field value for the cyclotron resonance signal B_r of BLG is not constant as a function of *n*, instead exhibiting rather complex variation. In Fig. 2(a), the T_4 and T_5 transitions gradually shift lower values when *n* approaches zero. For the two different channels of the T_3 transition presented in Fig. 2(b), B_r exhibits a sudden change to a lower

value near n = 0. Selected traces from Figs. 2(a) and 2(b) are presented in Appendix A. These shifts in B_r with respect to n is not predicted by the single-particle model (this model predicts that B_r is constant under variation of n). Therefore, we believe that the shift in B_r with n is an effect of many-body interactions in BLG. Similar changes in B_r with n have been reported in *h*-BN/MLG/*h*-BN and discussed in terms of many-body interactions [5,6]; our result is the first demonstration of an unambiguous signature of many-body interactions on BLG.

We measured V_{ph} versus B at the irradiation wavelengths of 10.675, 10.611, 10.275, 9.52, and 9.24 μm. For each wavelength, we examined two different n values, $n = 4.0 \times 10^{10}$ cm^{-2} and 1.55×10^{11} cm^{-2}, corresponding to the vicinity of the DP and away from the DP, respectively (indicated by red and black arrows, respectively in Fig. 2(b)); these results are plotted in Fig. 2(c) and traces are offset for clarity in the figure. Overall, both peaks in the double-peak structure of the T_3 transition shift with λ, as expected for CR. In addition, we found that the B_r for n values near to the DP (red line) are lower than those for n away from the DP (black line) for the same λ. The B_r values of the double-peak structures in Fig. 2(c) were extracted for two different n values, and these are plotted with respect to the irradiation energy E_{ph} as shown by the circles and the squares in Fig. 2(d). The LLs of BLG were calculated using the following equation [1]:

$$E_N = \frac{\mathrm{sgn}(N)}{\sqrt{2}}\left[(2|N|+1)\Delta^2 + \gamma_1^2 - \sqrt{\gamma_1^4 + 2(2|N|+1)\Delta^2\gamma_1^2 + \Delta^4}\right]^{1/2}, \quad (1)$$

where γ_1 is the interlayer coupling energy and $\Delta = \sqrt{2eBv_F\hbar}$. Here, v_F denotes the Fermi velocity, e the elementary charge, and $\hbar$ the reduced Planck constant. Then, the relationships between the transition energy and B_r for the two different channels in the T_3 transition (between $N = -2$ and $+3$, and between $N = -3$ and $+2$) were calculated, and these

are plotted in Fig. 2(d) as solid and dashed lines, respectively. We found that the experimentally obtained peak positions were in good agreement with eq. (1) plotted using the electron Fermi velocity $\upsilon_{F\text{-}e} = 1.137 \times 10^6$ m/s, hole Fermi velocity $\upsilon_{F\text{-}h} = 1.015 \times 10^6$ m/s, and $\gamma_1 = 0.39$ eV for the data in the vicinity of the DP (red lines). In contrast to this, for the data away from the DP, we found that using $\upsilon_{F\text{-}e} = 1.127 \times 10^6$ m/s, $\upsilon_{F\text{-}h} = 1.006 \times 10^6$ m/s, and $\gamma_1 = 0.39$ eV (black lines) resulted in good correspondence with the experimental data. Here, the different Fermi velocity values for the electrons and holes represent the electron–hole asymmetry of the band structure in BLG [1,20,21]. We assumed that the ratio $\upsilon_{F\text{-}e}/\upsilon_{F\text{-}h}$ and the value of γ_1 was constant for all the calculations. These comparisons allowed us to confirm our identification of BLG cyclotron resonances in the photothermoelectric measurements. In addition, we observed significantly different B_r values depending on the position of the E_F of BLG irrespective of the irradiation wavelength. The many-body interactions modify the energy splitting of the LLs, depending on the Fermi level, as illustrated in Fig. 2(e); when E_F is close to the DP, the spacing between the LLs increases as a result of many-body interactions [5,6]. The result shown here implies that for BLG there is a significant contribution from many-body interactions to the LLs that modify the energy splitting of the LLs due to the change of Fermi velocity depending on E_F. From the vertical offset between the straight lines in Fig. 2(d), the difference in the inter-LL spacing for the T_3 transitions (E_F close to the DP versus E_F away from the DP) is 2 meV.

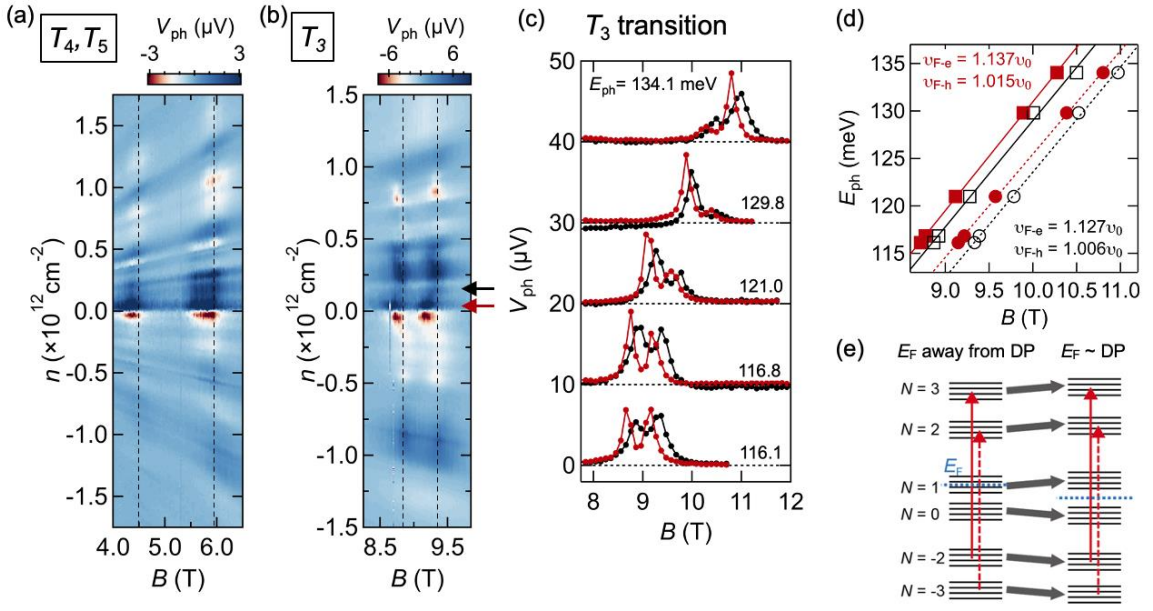

Figure 2. (a,b) Detailed mapping of V_{ph} as a function of magnetic field B and carrier density n at T = 2.0 K under irradiation at a wavelength λ of 10.675 μm for (a) T_4 and T_5 transitions, and (b) T_3 transition. (c) V_{ph} vs. B traces at selected λ (or E_{ph}). The red lines correspond to the case where Fermi energy E_F being located close to the Dirac point DP, while black lines correspond to E_F being away from the DP. Traces are offset for clarity and the baselines (corresponding to V_{ph} = 0) for each trace are indicated by the horisontal dashed lines. (d) Relationship between irradiation energy for the T_3 transition and the magnetic field value of the cyclotron resonance. Solid and dashed lines indicate calculated results for the energies of each transition based on eq. (1). In the figure, υ_0 is defined as 1×10^6 m/s. (e) Schematic energy level diagram illustrating the E_F dependence of cyclotron resonance transitions.

Detailed many-body interaction corrections of the LLs of BLG were recently calculated and reported by Shizuya [22]. Here, we compare our results with these theoretical calculations. To do this, V_{ph} data presented in Figs. 2(a) and 2(b) are plotted as a function of quantum Hall filling factor $\nu = hn/eB$ and magnetic field B, and the results are shown in Figs. 3(a) and 3(c), where h denotes the Planck constant. There are many of horizontal lines that appear along constant ν in Fig. 3(a) and 3(c). These are non-resonant background thermoelectric signal under irradiation. As far as the cyclotron resonance signal is sufficiently larger than this background signal, we can distinguish these two contributions (comparison between these contributions are presented in Appendix B). For comparison, the position of B_r expected from the theoretical calculation including many-body interaction is also presented in the Figs. 3(b) and 3(d) with respect to the number of filled Landau levels N_f. Since the calculation reported in ref. [22] was used to estimate the change of LL energies due to the many-body interaction contribution and normalized to the value obtained by neglecting many-body interaction effects, we converted the calculation result to the change of B_r by using eq. (1) (details of this conversion procedure is presented in Appendix C). Here, only the adjustment parameter is Fermi velocity of BLG without many-body interaction contribution υ_{F0}; we used this value to adjust the offset position of B_r presented in Fig. 3(b) and 3(d) to match with experiment, while relative change of B_r with respect to N_f does not significantly altered with this procedure. We also note that the definition of the filling factor ν in the experiment is not exactly the same as that of N_f as used in ref. [22]; $N_f = -2, -1, 0, +2, +3, +4$ can be considered to be equivalent to $\nu = -12, -8, -4, +4, +8$, and $+12$, respectively. However, $N_f = +1$ cannot be uniquely

associated with $\nu = 0$ because it is highly dependent on the valley and spin configuration of the lowest LLs of BLG ($N = 0$ and +1 in terms of the LL indices).

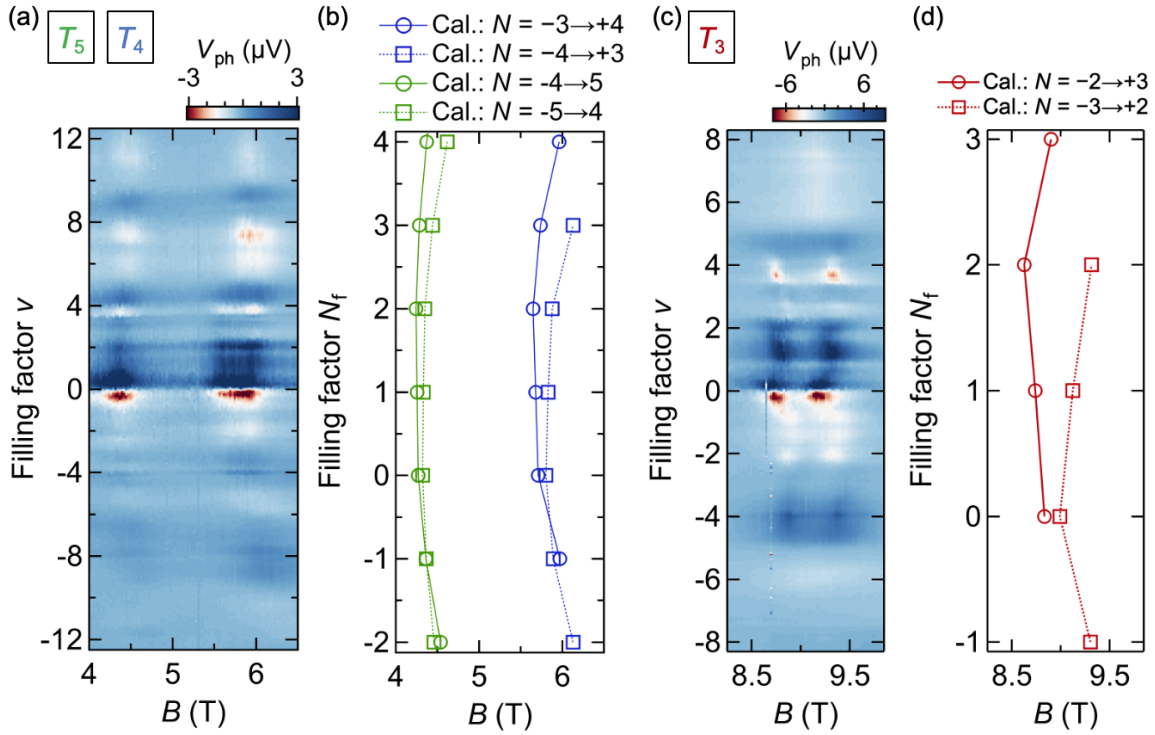

Figure 3. (a,c) Image plot of V_{ph} as a function of magnetic field B and quantum Hall filling factor ν at T = 2.0 K under irradiation at a wavelength λ of 10.675 μm for the (a) T_4 and T_5 transitions and (c) T_3 transition. (b,d) Positions of CR transition estimated from the theoretical calculation using a many-body correction for the (b) T_4 and T_5 transitions, and (d) T_3 transition plotted versus the number of filled Landau levels N_f. The theoretical calculation results are extracted from ref. [22].

We noticed several interesting differences and similarities between the experiment and calculation. First, the experimental results for the T_4 and T_5 transitions showed a decrease of B_r from high ν to $\nu = 0$. By contrast, the calculation results indicated the B_r decrease approaching $N_f = 0$ or +2 (corresponds to $\nu = -4$ and +4, respectively), depending on the transition channel. Although both experiment and calculation results in Figs. 3(a) and 3(b) showed that change of B_r exhibits convex to the left shape with similar ratios, the peak filling factors are different. Because of the different peak N_f positions for different channels, in the calculation, the splitting between the two different channels in the T_3 and T_4 transitions is larger for $N_f > 0$. In the experimental data, such a tendency is not obvious. Second, the experimental results for the T_3 showed a sharp reduction of B_r between $\nu = -1$ and +1, while the calculation results indicated the B_r gradually decrease approaching $N_f = 0$ or +2 similar to the T_4 and T_5 transitions. As we discussed in Fig. 2, this sharp reduction of B_r in the experiment corresponds to the increase of energy separation of LLs between $\nu = -1$ and +1, and such sharp change in the calculated results is not discussed in ref. [22]. Although the origin of these above-mentioned discrepancy between the experimental and theoretical data is not clear at this moment, we suggest that our results indicate that the detail of the LL structure plays an important role in determining the electronic behavior of BLG. We note that the detailed sequence of LLs (spin, valley, and orbit) may be different between experiment and theory. The calculations were made assuming a valley-dominant sequence in LLs, while we could not confirm the exact LL sequence in our device. The LL sequence in the range of $\nu = -4$ to +4 is sensitive to various parameters, such as interlayer bias and magnetic field; this could be the origin of the difference between the results obtained using our device and the calculation results presented in ref. [22]. Our results may

stimulate further theoretical work aimed at obtaining a complete understanding of the effects of many-body interactions in BLG.

In summary, we demonstrated cyclotron resonances in *h*-BN/BLG/*h*-BN structures via photothermoelectric measurements under infrared laser irradiation. This method enables the detection of multiple cyclotron resonance transitions as the value of E_F for BLG is varied. The magnetic field value for the cyclotron resonance underwent a non-negligible shift when the E_F of BLG approached the DP. We attribute this to a many-body interaction effect occurring in the high-quality BLG. Our results revealed a significant contribution of many-body interaction effects to the CR of BLG and provide an effective method for probing these interaction effects in graphene heterostructures.

Acknowledgements

The authors gratefully acknowledge Prof. Ken-ichi Shizuya for discussion on many-body interaction theory of bilayer graphene. This work was supported by the CREST and Mirai programs of the Japan Science and Technology Agency (JST) (grant numbers JPMJCR15F3, JPMJCR20B4, and JPMJMI21G9), KAKENHI grants from the Japan Society for the Promotion of Science (JSPS) (grant numbers JP19H02542, JP19H01820, JP20H00127, JP20H00354, JP21H05232, JP21H05233, and JP21H05234), and World-leading Innovative Graduate Study Program for Materials Research, Information, and Technology (MERIT-WINGS) of the University of Tokyo.

Appendix A: Detail of photovoltage data for T_3, T_4, and T_5 CR transitions

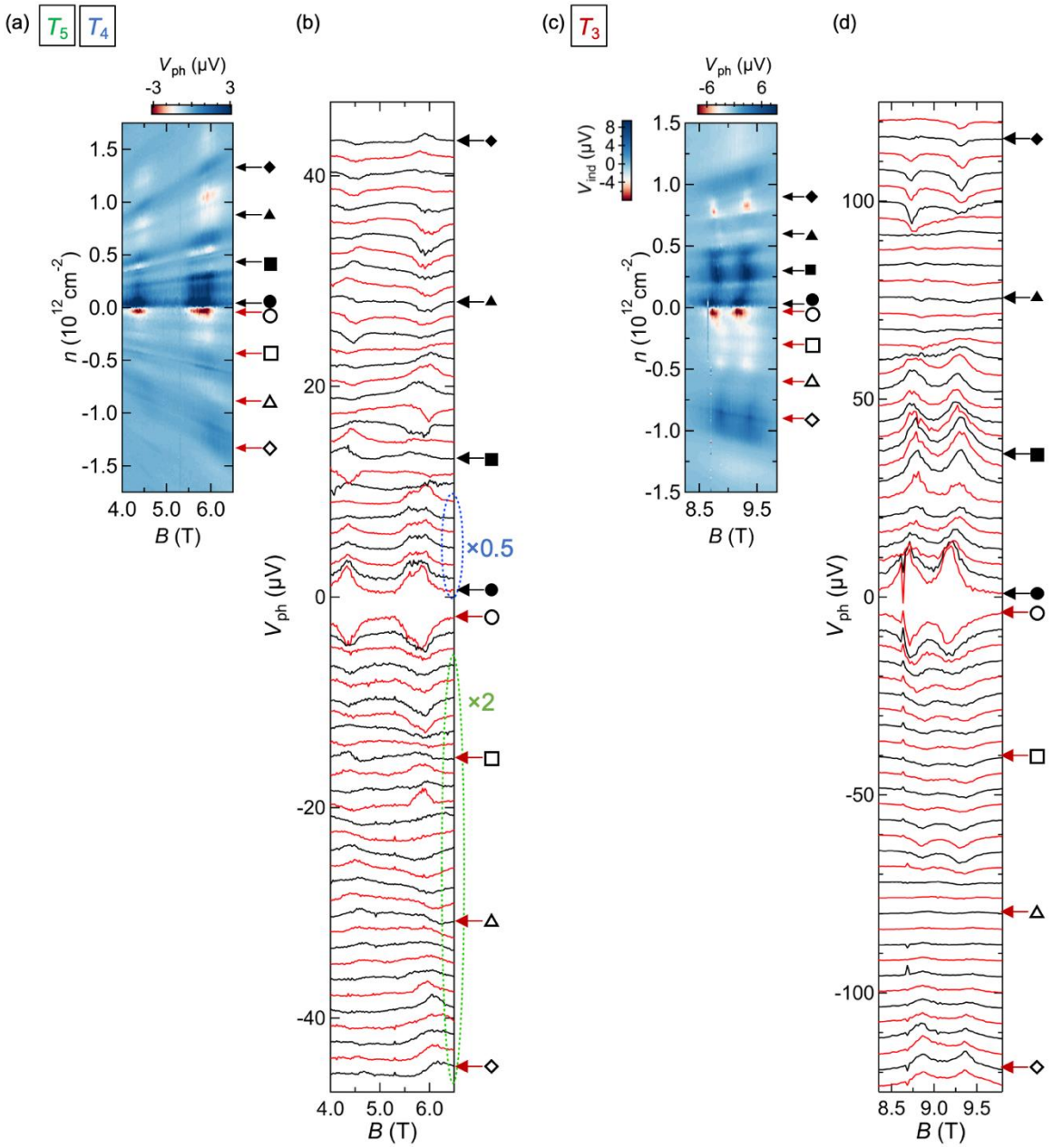

Figure A1. (a,c) Detailed mapping of V_{ph} as a function of magnetic field B and carrier density n at T = 2.0 K under irradiation at a wavelength λ of 10.675 μm for the (a) T_4 and T_5 transitions and (c) T_3 transition. (b,d) V_{ph} vs. B traces at selected n values for (b) the T_4 and T_5 transitions and (d) the T_3 transition. The corresponding n values are indicated by circles, squares, triangles, and diamonds in panels (a) and (c). The traces

are offset for clarity, and those indicated by blue and green dashed circles are multiplied by a factor of 0.5 and 2.0, respectively.

Appendix B: Comparison between cyclotron resonance signal and background signal

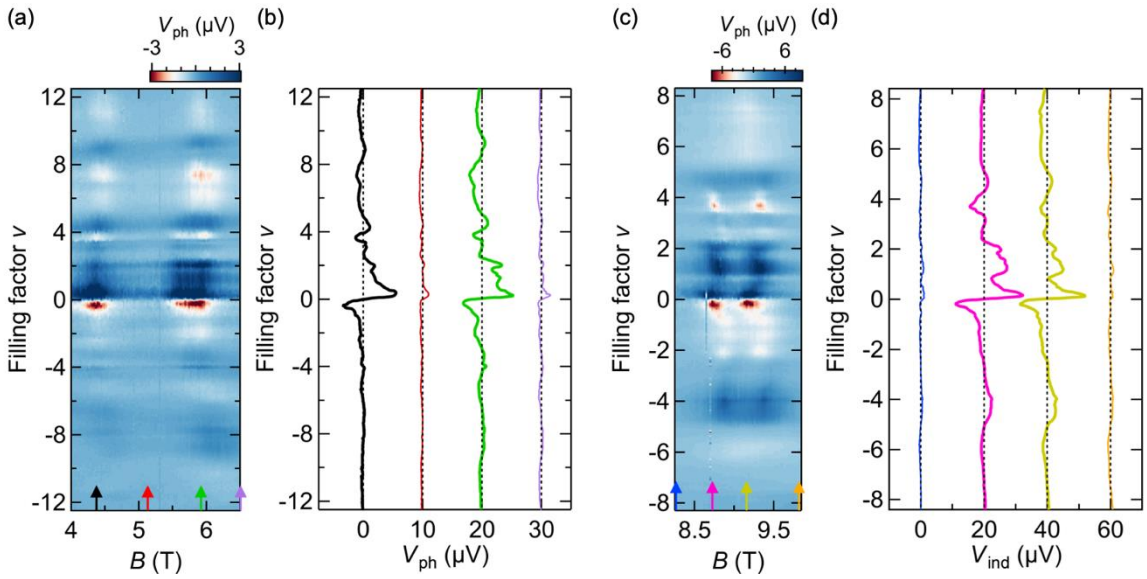

Figure A2. (a,c) Image plot of V_{ph} as a function of magnetic field B and quantum Hall filling factor ν at T = 2.0 K under irradiation at a wavelength λ of 10.675 μm for the (a) T_4 and T_5 transitions and (c) T_3 transition. (b,d) Cross-section of panels (a,c) at constant B. The corresponding B values are indicated by arrows in panel (a,c). The traces shown by thick lines are data at the cyclotron resonance and thin lines are the data corresponds to the back ground non-resonant thermoelectric signal.

Appendix C: Extraction of relationship between B_r and N_f from theoretical calculation

In the theoretical calculation reported by Shizuya [22], the change of LL energies due to the many-body interaction contribution was estimated and results are normalized to the value obtained by neglecting many-body interaction effects. The magnetic field value used for the calculation was B = 20 T, the interlayer bias u was zero, and $\tilde{V}_c/\omega_c = 0.4$ was used for the strength of the Coulomb interaction $\tilde{V}_c$ normalized to the cyclotron energy for monolayer graphene ω_c [22-24]; here, ω_c is used as a basic cyclotron energy. Using eq.(1), the change of energy is first converted to the change of Fermi velocity; here we used γ_1 = 0.39 eV and constant $\upsilon_{F\text{-}e}/\upsilon_{F\text{-}h}$ ratio throughout the analysis. Thus, we used $\upsilon_{F\text{-}e} = \upsilon_F$ for electrons and $\upsilon_{F\text{-}h} = 0.892 \times \upsilon_F$ for holes. We set the LL energies of T_3, T_4, and T_5 transitions neglecting many-body interaction effects as 0.2, 0.285, and 0.36 eV, respectively. These are corresponding to the Fermi velocity without many-body interaction υ_{F0} of 1.035×10^6, 1.041×10^6 m/s, and 1.045×10^6 m/s, respectively. Next, by fixing the value of E_N in eq. (1) as E_{ph} at λ = 10.675 μm (E_{ph} = 116.14 meV), it was possible to convert the Fermi velocity into B_r value via eq. (1) and extracted B_r was plotted in Figs. 3(b) and 3(d). The theoretical calculations were concerned how the LL energy spacing changes with the number of filled LLs below E_F because of the interaction effect. Therefore, we believe that the relative change in the LLs with respect to N_f is not significantly altered by this conversion, which allows us to make a reasonable comparison between experiment and B_r extracted from the theoretical calculation.

References

[1] E. A. Henriksen, Z. Jiang, L. C. Tung, M. E. Schwartz, M. Takita, Y. J. Wang, P. Kim, and H. L. Stormer, Phys. Rev. Lett. **100**, 087403 (2008).

[2] R. S. Deacon, K. C. Chuang, R. J. Nicholas, K. S. Novoselov, and A. K. Geim, Phys. Rev. B **76**, 081406 (2007).

[3] K. Kinoshita, R. Moriya, M. Arai, S. Masubuchi, K. Watanabe, T. Taniguchi, and T. Machida, Appl. Phys. Lett. **113**, 103102 (2018).

[4] K. Kinoshita, R. Moriya, S. Masubuchi, K. Watanabe, T. Taniguchi, and T. Machida, Appl. Phys. Lett. **115**, 153102 (2019).

[5] B. J. Russell, B. Zhou, T. Taniguchi, K. Watanabe, and E. A. Henriksen, Phys. Rev. Lett. **120**, 047401 (2018).

[6] J. Sonntag, S. Reichardt, L. Wirtz, B. Beschoten, M. I. Katsnelson, F. Libisch, and C. Stampfer, Phys. Rev. Lett. **120**, 187701 (2018).

[7] M. Onodera, M. Arai, S. Masubuchi, K. Kinoshita, R. Moriya, K. Watanabe, T. Taniguchi, and T. Machida, Nano Lett. **19**, 8097 (2019).

[8] M. Onodera, K. Kinoshita, R. Moriya, S. Masubuchi, K. Watanabe, T. Taniguchi, and T. Machida, Nano Lett. **20**, 4566 (2020).

[9] I. O. Nedoliuk, S. Hu, A. K. Geim, and A. B. Kuzmenko, Nat. Nanotechnol. **14**, 756 (2019).

[10] Z. Jiang, E. A. Henriksen, L. C. Tung, Y. J. Wang, M. E. Schwartz, M. Y. Han, P. Kim, and H. L. Stormer, Phys. Rev. Lett. **98**, 197403 (2007).

[11] J. Pack, B. J. Russell, Y. Kapoor, J. Balgley, J. Ahlers, T. Taniguchi, K. Watanabe, and E. A. Henriksen, Phys. Rev. X **10**, 041006 (2020).

[12] K. Shizuya, Phys. Rev. B **98**, 115419 (2018).

[13] W. Kohn, Phys. Rev. **123**, 1242 (1961).

[14] R. E. Throckmorton and S. Das Sarma, Phys. Rev. B **98**, 155112 (2018).

[15] A. S. Mayorov, D. C. Elias, M. Mucha-Kruczynski, R. V. Gorbachev, T. Tudorovskiy, A. Zhukov, S. V. Morozov, M. I. Katsnelson, A. K. Geim, and K. S. Novoselov, Science **333**, 860 (2011).

[16] L. Ju, L. Wang, X. Li, S. Moon, M. Ozerov, Z. Lu, T. Taniguchi, K. Watanabe, E. Mueller, F. Zhang, D. Smirnov, F. Rana, and P. L. Mceuen, Nat. Commun. **11**, 2941 (2020).

[17] X. Xu, N. M. Gabor, J. S. Alden, A. M. Van Der Zande, and P. L. Mceuen, Nano Lett. **10**, 562 (2010).

[18] N. M. Gabor, J. C. W. Song, Q. Ma, N. L. Nair, T. Taychatanapat, K. Watanabe, T. Taniguchi, L. S. Levitov, and P. Jarillo-Herrero, Science **334**, 648 (2011).

[19] K. J. Tielrooij, M. Massicotte, L. Piatkowski, A. Woessner, Q. Ma, P. Jarillo-Herrero, N. F. V. Hulst, and F. H. L. Koppens, J. Phys.: Condens. Matter **27**, 164207 (2015).

[20] K. Zou, X. Hong, and J. Zhu, Phys. Rev. B **84**, 085408 (2011).

[21] L. M. Zhang, Z. Q. Li, D. N. Basov, M. M. Fogler, Z. Hao, and M. C. Martin, Phys. Rev. B **78**, 235408 (2008).

[22] K. Shizuya, Phys. Rev. B **101**, 195429 (2020).

[23] B. M. Hunt, J. I. A. Li, A. A. Zibrov, L. Wang, T. Taniguchi, K. Watanabe, J. Hone, C. R. Dean, M. Zaletel, R. C. Ashoori, and A. F. Young, Nat. Commun. **8**, 948 (2017).
[24] K. Shizuya, Phys. Rev. B **81**, 075407 (2010).